



Improvement of tap density of $\text{TiO}_2(\text{B})$ powder as high potential negative electrode for lithium ion batteries



Morihiro Saito, Yoshiyuki Nakano, Mikihiro Takagi, Naoki Honda, Akimasa Tasaka, Minoru Inaba*

Department of Molecular Chemistry and Biochemistry, Faculty of Science and Engineering, Doshisha University, Kyotanabe, Kyoto 610-0321, Japan

HIGHLIGHTS

- The morphology of $\text{TiO}_2(\text{B})$ powder were controlled using large-size Nb-doped rutile TiO_2 .
- The tap density of Nb-doped samples was improved by a factor of 2.
- The discharge capacity per electrode volume was significantly improved by Nb-doping.

ARTICLE INFO

Article history:

Received 20 November 2012

Received in revised form

26 February 2013

Accepted 13 April 2013

Available online 8 May 2013

Keywords:

$\text{TiO}_2(\text{B})$

Nb-doping

High potential negative electrode

High tap density

ABSTRACT

To improve the tap density of $\text{TiO}_2(\text{B})$ as a high potential negative electrode for lithium-ion batteries, the particle size and the shape of the $\text{TiO}_2(\text{B})$ were controlled by a new synthetic method using large-size Nb-doped rutile TiO_2 as a starting material. The Nb-doped $\text{TiO}_2(\text{B})$ particles, $\text{Ti}_{0.93}\text{Nb}_{0.07}\text{O}_2(\text{B})$ and $\text{Ti}_{0.90}\text{Nb}_{0.10}\text{O}_2(\text{B})$, were much smaller (diameter: ca. 100 nm, length: ca. 800 nm) than the conventional $\text{TiO}_2(\text{B})$ prepared using fine anatase TiO_2 particles as a starting material, and were aggregated to form secondary particles with a diameter of 3–30 μm . The tap densities of $\text{Ti}_{0.93}\text{Nb}_{0.07}\text{O}_2(\text{B})$ and $\text{Ti}_{0.90}\text{Nb}_{0.10}\text{O}_2(\text{B})$ were successfully high (0.77 and 0.66 g cm^{-3} , respectively), which were ca. 2-fold higher than that of the conventional $\text{TiO}_2(\text{B})$ (0.30 g cm^{-3}). As a result, the discharge capacity per electrode volume was significantly improved for both Nb-doped samples without sacrificing the cycleability. Non-doped $\text{TiO}_2(\text{B})$ was prepared from large-size rutile TiO_2 by a similar method, but it deteriorated upon cycling, accompanied by the formation of the anatase phase. It was shown that Nb-doping not only improves the discharge capacity per electrode volume, but also effectively stabilizes the $\text{TiO}_2(\text{B})$ crystal structure of the small particles.

© 2013 Elsevier B.V. All rights reserved.

1. Introduction

In recent years, large-format lithium-ion batteries (LIBs) have attracted much attention for use in hybrid vehicle, electric vehicles and energy storages. However, there remain serious problems, such as safety, durability, and cost, to be solved before commercialization [1]. The use of high potential negative electrodes working at potentials higher than 1.0 V vs. Li/Li⁺ is one of the ways for solving these issues [2–15], though it sacrifices the energy density of the resulting batteries. Spinel type $\text{Li}_4\text{Ti}_5\text{O}_{12}$ (hereafter denoted as LTO) has a very flat potential plateau at around 1.55 V vs. Li/Li⁺ with good reversibility and structural stability during the charge and

discharge processes [2,3], and is therefore one of the promising candidates for high potential negative electrodes of the large-format LIBs. However, the charge/discharge capacity of LTO is limited by the theoretical one (175 mAh g⁻¹), which is unfavorably lower than that of graphite (372 mAh g⁻¹). Another promising candidate as a high potential negative electrode is $\text{TiO}_2(\text{B})$, which is a polymorph of TiO_2 [7–18]. Armstrong et al. reported that the nanowires [7–9,15] and nanotubes [10,11] of $\text{TiO}_2(\text{B})$, which were prepared by a hydrothermal method, exhibited high reversible capacity (305 mAh g⁻¹ and 330 mAh g⁻¹, respectively) close to the theoretical one (335 mAh g⁻¹) with good cycleability. We have prepared $\text{K}_2\text{Ti}_4\text{O}_9$ and $\text{Cs}_2\text{Ti}_5\text{O}_{11}$ precursors by a solid state reaction, and obtained micrometer-size $\text{TiO}_2(\text{B})$ powder after ion-exchange to protons, and dehydration at 500 °C [16–18]. The $\text{TiO}_2(\text{B})$ powder, especially prepared from the $\text{Cs}_2\text{Ti}_5\text{O}_{11}$ precursor, exhibited a reversible capacity of 314.4 mAh g⁻¹ and a good cycleability (287.9 mAh g⁻¹ in the 50th cycle) between 1.4 and 3.0 V at a C/6 rate

* Corresponding author. Tel.: +81 774 65 6591; fax: +81 774 65 6841.

E-mail addresses: minaba@mail.doshisha.ac.jp, [\(M. Inaba\).](mailto:inaba19610923@gmail.com)

[18]. However, the $\text{TiO}_2(\text{B})$ powder still have problems such as low tap density owing to the needle-shape, which leads to a low practical capacity per volume of the electrode.

As we reported previously, the shape of the $\text{TiO}_2(\text{B})$ powder is determined by the shape of the alkali metal titanate precursors [18], and it is therefore important to optimize the shape and size of the precursor in order to improve the tap density. We have so far investigated the effects of Nb-doping to $\text{TiO}_2(\text{B})$ aiming at improving the electronic conductivity as reported for LTO [19], and we accidentally found that the Nb-doping has a pronounced effect on the shape and size of the resulting Nb-doped $\text{TiO}_2(\text{B})$ particles. In this study, we prepared Nb-doped $\text{TiO}_2(\text{B})$ using Nb-doped rutile TiO_2 as a starting material, and investigated the effects of Nb-doping on the shape and size of the resulting Nb-doped $\text{TiO}_2(\text{B})$ particles and their electrochemical properties as negative electrodes in LIBs.

2. Experimental

2.1. Synthesis and characterization of Nb-doped $\text{TiO}_2(\text{B})$

Anatase TiO_2 (Aldrich, ≥99%, average diameter: 100 nm) and Nb_2O_5 (Aldrich, 99.9%, under 325 mesh) powders were mixed and fired at 1350 °C for 10 h in air to obtain $\text{Ti}_{1-x}\text{Nb}_x\text{O}_2$ ($x = 0.07$ or 0.10) powder as a starting material. The Nb-doped TiO_2 powder was mixed with K_2CO_3 (Wako Pure Chemicals, 99.8%) at a molar ratio of 1:4, and fired at 900 °C for 24 h in air to obtain $\text{K}_2\text{Ti}_{4(1-x)}\text{Nb}_{4x}\text{O}_9$ precursor ($x = 0.07$ or 0.10) [16–18]. After the K^+ ions in the precursor were exchanged to protons in 1 M HCl for 3 days, the resulting protonated powder was filtered, and dehydrated at 500 °C for 30 min in air, and $\text{Ti}_{1-x}\text{Nb}_x\text{O}_2(\text{B})$ ($x = 0.07$ or 0.10) powder was obtained.

The conventional $\text{TiO}_2(\text{B})$ powder prepared using the fine anatase TiO_2 as a starting material [16–18] were used for comparison. In some experiments, a non-doped rutile TiO_2 was prepared from the anatase TiO_2 by heating at 1350 °C for 10 h in air, and non-doped $\text{TiO}_2(\text{B})$ powder was obtained using the rutile TiO_2 as a starting material to investigate the effects of Nb-doping. In both cases, the procedures for precursor preparation, ion-exchange, and dehydration were the same as described above.

The Nb-doped and non-doped $\text{TiO}_2(\text{B})$ samples were analyzed by X-ray diffraction (XRD, Rigaku, RINT2000) using a $\text{Cu K}\alpha$ radiation (40 kV, 200 mA), and by field-emission scanning electron microscopy (FE-SEM, JEOL, JSM7001FD) at an accelerating voltage of 5–15 kV.

The tap density was measured as follows: A given amount of the Nb-doped or non-doped $\text{TiO}_2(\text{B})$ powder was weighed, and put into a graduated cylinder (10 mL). The graduated cylinder was tapped a few thousand times by hand, and measured the volume of the powder. The tap density was calculated using the volume and weight of the powder.

2.2. Charge and discharge tests

The $\text{TiO}_2(\text{B})$ powder was mixed with Ketjen Black (KB, Lion Corp., EC600JD) as a conductor and poly(vinylidene fluoride) (PVDF, Kureha, KF Polymer) as a binder at a weight ratio of 8:1:1 using 1-methyl-2-pyrrolidinone (Wako Pure Chemicals, reagent grade) as a solvent to make a viscous slurry. The slurry was coated on a copper-foil current collector with a thickness of 100 μm . After dried, the electrode composite layer (30–40 μm in thickness) was then roll-pressed to 20 μm . The loading of the active material on the Cu foil was in the range of 2.0–2.5 mg cm^{-2} . Composite electrode disks (1.77 cm^2) were punched out from the foil, and dried overnight at 80 °C under vacuum before use.

A coin-type two-electrode half-cell was constructed from the $\text{TiO}_2(\text{B})$ composite disk electrode, a separator (Celgard® 2400) and

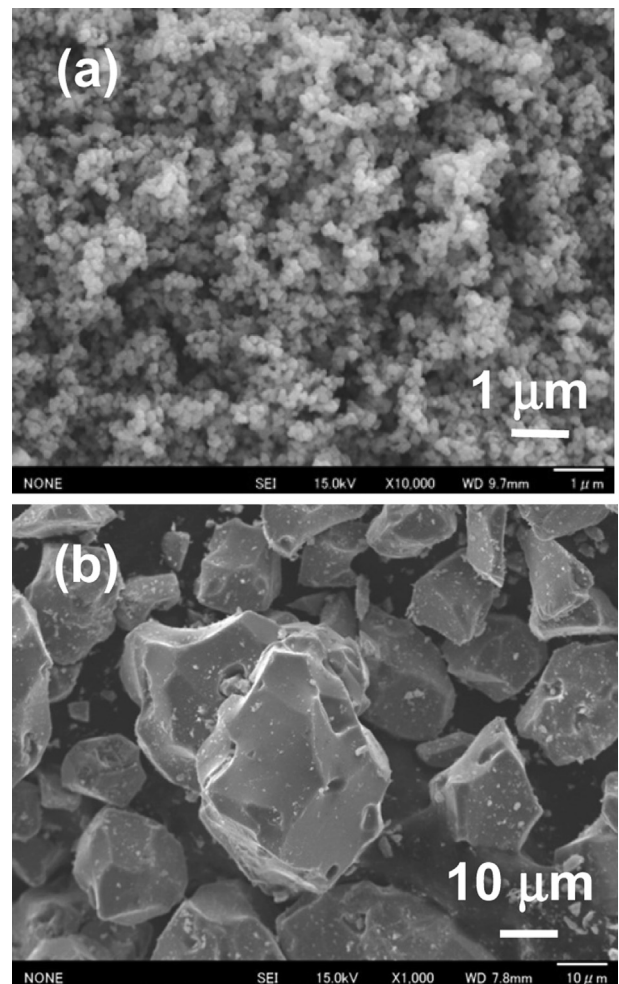


Fig. 1. SEM images of (a) anatase TiO_2 and (b) Nb-doped TiO_2 ($\text{Ti}_{0.93}\text{Nb}_{0.07}\text{O}_2$) powder as starting materials.

a lithium-foil counter electrode (Honjo Metal, 0.5 mm in thickness) in an argon-filled glove box (Miwa, MDB-1B + MM3-P60S) with a dew point lower than –60 °C. 1.0 M LiPF_6 dissolved in 1:1 mixture (by volume) of ethylene carbonate (EC) + diethyl

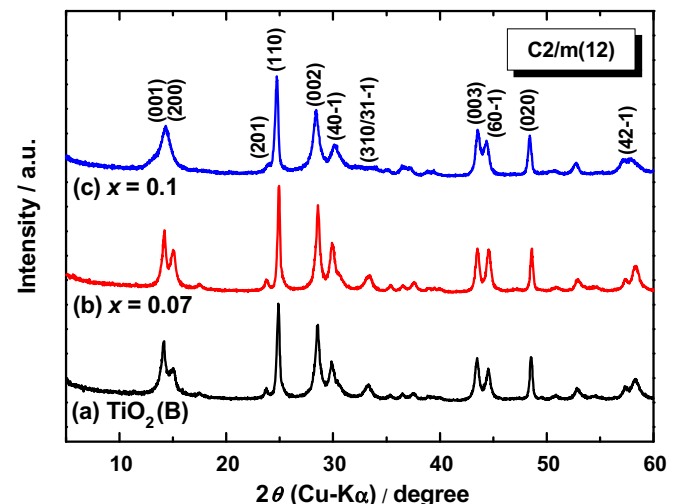


Fig. 2. XRD patterns of (a) $\text{TiO}_2(\text{B})$ powder prepared by the conventional method using anatase TiO_2 as a starting material and (b, c) $\text{Ti}_{1-x}\text{Nb}_x\text{O}_2(\text{B})$ ($x = 0.07, 0.10$) samples prepared from Nb-doped rutile TiO_2 as a starting material.

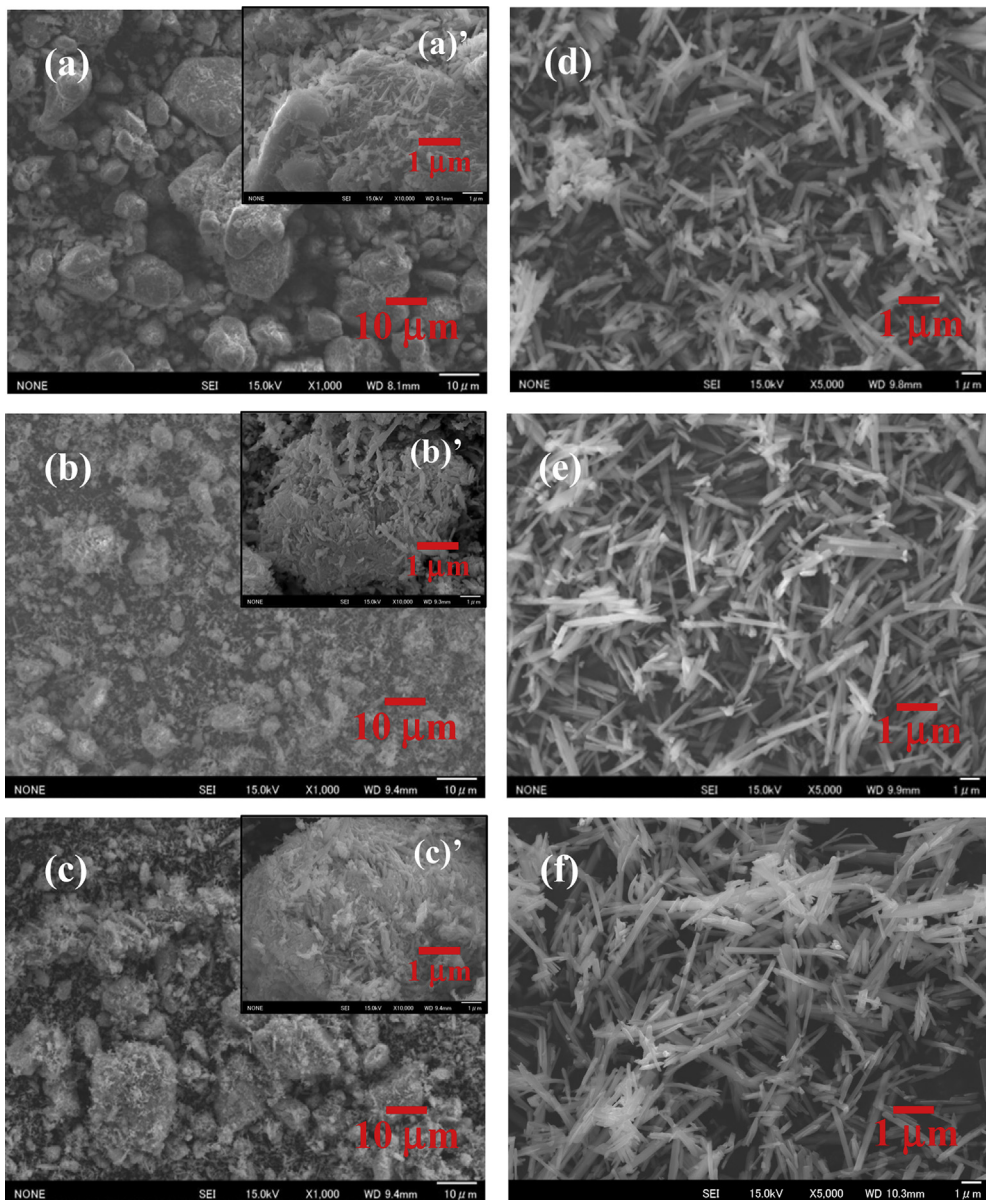


Fig. 3. SEM images of (a) K₂Ti_{3.72}Nb_{0.28}O₉, (b) H₂Ti_{3.72}Nb_{0.28}O₉, (c) Ti_{0.93}Nb_{0.07}O₂(B) particles prepared from Nb-doped rutile TiO₂ particles (d) K₂Ti₄O₉, (e) H₂Ti₄O₉ and (f) TiO₂(B) prepared by the conventional method using anatase TiO₂ particles as a starting material. The inserted SEM images of (a)', (b)' and (c)' are magnified ones for (a), (b) and (c), respectively.

carbonate (DEC) was used as an electrolyte solution. Charge and discharge characteristics were measured between 1.4 and 3.0 V at a C/6 rate at 30 °C using a battery test system (Hokuto Denko, HJ1001SM8). In the present study, lithium-ion insertion into and extraction from TiO₂(B) are denoted as charging and discharging, respectively, considering the role of TiO₂(B) as a negative electrode in LIBs.

3. Results and discussion

3.1. Characterizations of the Nb-doped TiO₂(B) powders

Fig. 1 shows SEM images of the anatase TiO₂ powder and the Nb-doped TiO₂ (Ti_{0.93}Nb_{0.07}O₂) powder used as the starting materials for the preparation of the conventional and Nb-doped TiO₂(B) samples, respectively. The anatase TiO₂ powder was very fine, and its particle size was ca. 100 nm. The Ti_{1-x}Nb_xO₂ ($x = 0.07$ and 0.10) powder had a rutile structure, and the particle size was large (10–30 μm). The color

of the Ti_{1-x}Nb_xO₂ was bluish black, which indicated that the valence of Nb ions was +5 and part of Ti⁴⁺ was reduced to Ti³⁺ in Ti_{1-x}Nb_xO₂. However, the color changed from bluish black to white after the ion-exchange process, and did not change after the dehydration process at 500 °C. It is therefore speculated that the valences of Ti and Nb ions were +4 in Nb-doped TiO₂(B), and an enhancement in electronic conductivity by Nb-doping would be negligible in the charge and discharge tests described later.

Fig. 2 shows the XRD patterns of the conventional TiO₂(B) and Ti_{1-x}Nb_xO₂(B) ($x = 0.07$ and 0.10) samples [1–3]. Both Nb-doped samples showed similar XRD patterns to the conventional TiO₂(B) powder, but each peak shifted to a slightly lower angle. These facts indicated that the Nb-doped samples were a single phase of the TiO₂(B) structure and the doped Nb⁴⁺ ions (ionic radius: 68.0 pm) substituted to the Ti⁴⁺ (ionic radius: 60.5 pm) sites in the TiO₂(B) structure.

Fig. 3 shows SEM images of the precursors, protonated precursors and dehydrated samples obtained at each synthetic stage

Table 1

Average sizes (diameter/length), tap densities, electrode densities, 1st discharge capacities, and Coulombic efficiencies of the conventional $\text{TiO}_2(\text{B})$ prepared anatase TiO_2 , and $\text{Ti}_{1-x}\text{Nb}_x\text{O}_2(\text{B})$ ($x = 0.07$ and 0.10) and $\text{TiO}_2(\text{B})$ prepared from rutile $\text{Ti}_{1-x}\text{Nb}_x\text{O}_2$ and TiO_2 powder, respectively.

Samples	Conventional $\text{TiO}_2(\text{B})$	$\text{Ti}_{0.93}\text{Nb}_{0.07}\text{O}_2(\text{B})$	$\text{Ti}_{0.90}\text{Nb}_{0.10}\text{O}_2(\text{B})$	$\text{TiO}_2(\text{B})$
TiO ₂ raw material	Anatase TiO_2	Rutile $\text{TiO}_{0.93}\text{Nb}_{0.07}\text{O}_2$	Rutile $\text{TiO}_{0.90}\text{Nb}_{0.10}\text{O}_2$	Rutile TiO_2
Average diameter/length (nm)	250/2000	100/800	100/800	100/800
Tap density (g cm ⁻³)	0.30	0.77	0.66	0.67
Electrode density (g cm ⁻³)	0.92	1.21	1.12	1.01
1 st discharge capacity per weight (mAh g ⁻¹) ^a	190	184	201	200
1 st discharge capacity per volume (mAh cm ⁻³) ^b	175	223	225	202
Coulombic efficiency in the first cycle (mAh g ⁻¹) ^a	30	38	27	45

^a Based on the weight of the active material only.

^b Based on the volume of the electrode including the binder and the conductor.

for the $\text{Ti}_{0.93}\text{Nb}_{0.07}\text{O}_2(\text{B})$ and the conventional $\text{TiO}_2(\text{B})$ samples. The conventional $\text{TiO}_2(\text{B})$ powder prepared from fine anatase TiO_2 powder (Fig. 3(f)) had a relatively large needle-like structure with a length of ca. 2 μm and a diameter of ca. 250 nm. The shape, the needle-like structure, is characteristic of the $\text{K}_2\text{Ti}_4\text{O}_9$ precursor (Fig. 3(d)), and did not change appreciably after the ion-exchange and dehydration processes. The needle-like structure of the precursor was fully developed by the use of the fine anatase TiO_2 powder as a starting material.

When the Nb-doped rutile TiO_2 as a starting material, the morphology of the powder at each stage were totally different. At a glance of Fig. 3(a), the precursor of the Nb-doped $\text{TiO}_2(\text{B})$ ($\text{K}_2\text{Ti}_{3.72}\text{Nb}_{0.28}\text{O}_9$) seemed large particles with a diameter of 3–30 μm . However, a closer look revealed that these large particles were aggregated secondary particles consisting of very fine primary particles of $\text{K}_2\text{Ti}_{3.72}\text{Nb}_{0.28}\text{O}_9$. This fact clearly indicates that K^+ ions from K_2CO_3 (or K_2O) penetrated into the large Nb-doped rutile TiO_2 particles and the fine precursor particles were formed inside. The shape and size of the powder did not change appreciably after the ion-exchange (Fig. 3(b)) and dehydration processes (Fig. 3(c)). The primary particles of the resulting $\text{Ti}_{0.93}\text{Nb}_{0.07}\text{O}_2(\text{B})$ particles also had a needle-like structure, but their size was much smaller than that of the conventional $\text{TiO}_2(\text{B})$. The average diameter and length of the primary particles were ca. 100 nm and 800 nm, respectively. Similar results were obtained for the $\text{Ti}_{0.90}\text{Nb}_{0.10}\text{O}_2(\text{B})$ powder. The tap densities of the conventional $\text{TiO}_2(\text{B})$ and the Nb-doped $\text{TiO}_2(\text{B})$ samples and the densities of the composite electrodes prepared from these samples are shown in Table 1. While the tap density of the conventional $\text{TiO}_2(\text{B})$ powder was very low (0.30 g cm⁻³), it was doubled for $\text{Ti}_{0.93}\text{Nb}_{0.07}\text{O}_2(\text{B})$ and $\text{Ti}_{0.90}\text{Nb}_{0.10}\text{O}_2(\text{B})$ (0.77 and 0.66 g cm⁻³, respectively). The high tap densities of the $\text{Ti}_{0.93}\text{Nb}_{0.07}\text{O}_2(\text{B})$ and $\text{Ti}_{0.90}\text{Nb}_{0.10}\text{O}_2(\text{B})$ samples resulted in higher electrode densities (1.21 and 1.12 g cm⁻³, respectively) than that of the conventional $\text{TiO}_2(\text{B})$ (0.92 g cm⁻³) as shown in Table 1.

3.2. Electrochemical properties of the Nb-doped $\text{TiO}_2(\text{B})$

Fig. 4 compares charge and discharge curves of the conventional $\text{TiO}_2(\text{B})$ and the Nb-doped $\text{TiO}_2(\text{B})$ samples in 1 M $\text{LiPF}_6/\text{EC} + \text{DEC}(1:1)$. All the samples showed plateaux at ca. 1.6 V vs. Li/Li^+ on the charge and discharge curves, which is characteristic of $\text{TiO}_2(\text{B})$. Almost no difference in the shape of charge and discharge curves was observed between the conventional $\text{TiO}_2(\text{B})$ and the Nb-doped samples. The discharge capacities based on the weight and the volume of these samples as well as Coulombic efficiencies

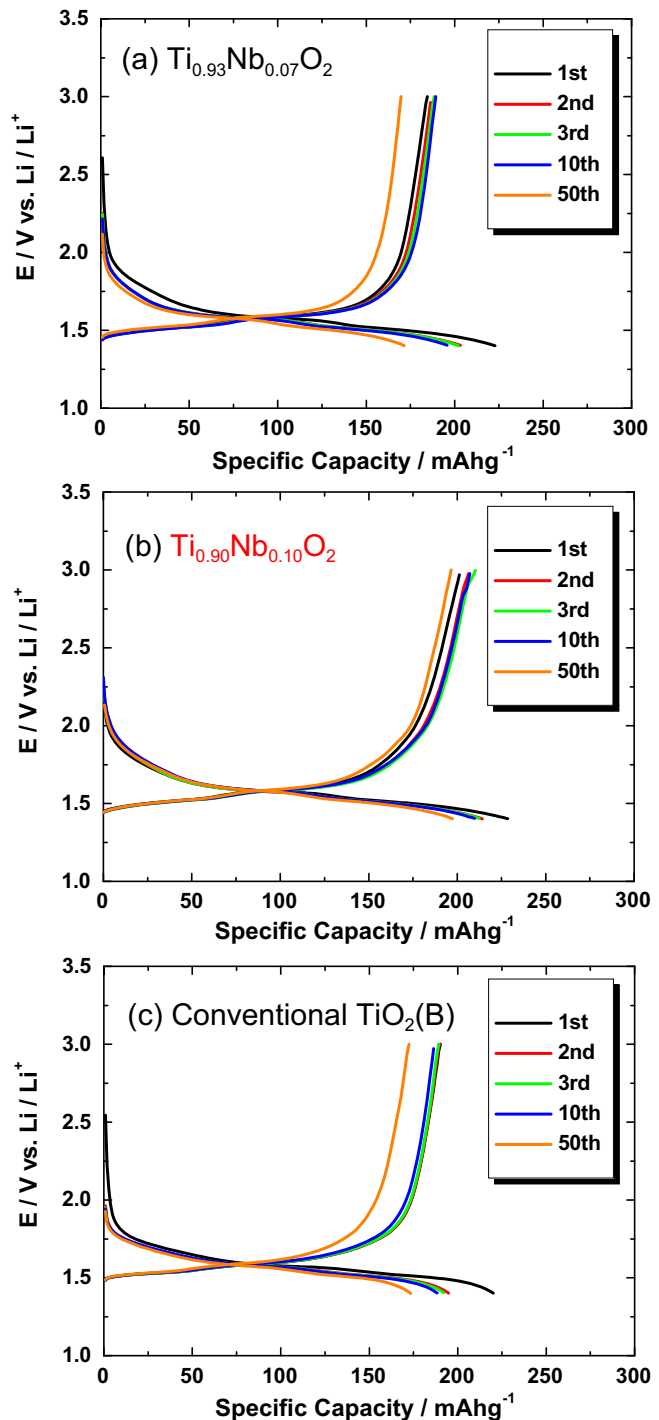


Fig. 4. Charge and discharge curves of (a) $\text{Ti}_{0.93}\text{Nb}_{0.07}\text{O}_2$, (b) $\text{Ti}_{0.90}\text{Nb}_{0.10}\text{O}_2$, and (c) The conventional $\text{TiO}_2(\text{B})$ samples between 1.4 and 3.0 V at C/6 in 1 M $\text{LiPF}_6/\text{EC} + \text{DEC}(1:1)$.

in the first cycle are summarized in Table 1. The Nb-doped samples exhibited discharge capacities per weight comparable with or slightly higher than that of the conventional $\text{TiO}_2(\text{B})$, even though the Nb-doped samples have reduced theoretical capacities owing to the presence of inactive Nb^{4+} ions. This may be due to the smaller particle size of the Nb-doped samples.

In contrast, the discharge capacity per electrode volume was greatly influenced by Nb-doping. The discharge capacity per electrode volume for the conventional $\text{TiO}_2(\text{B})$ was 175 mAh cm⁻³, but those for $\text{Ti}_{0.93}\text{Nb}_{0.07}\text{O}_2(\text{B})$ and $\text{Ti}_{0.90}\text{Nb}_{0.10}\text{O}_2(\text{B})$ were 223 and 225 mAh cm⁻³, respectively. The increase in the discharge capacity

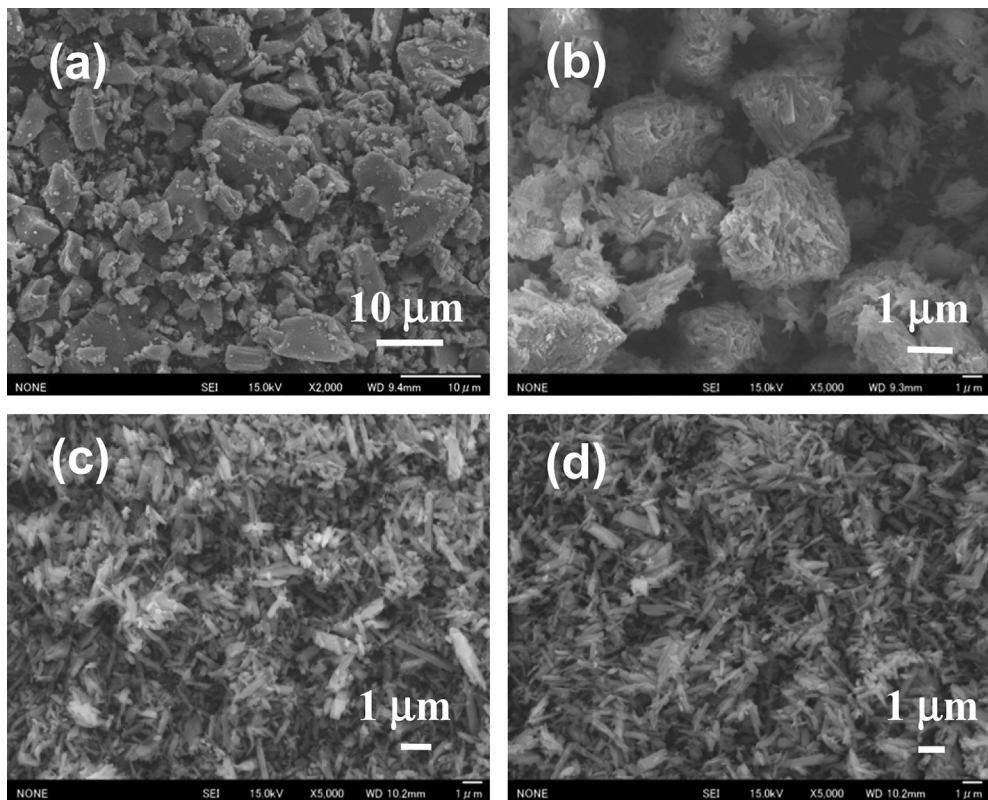


Fig. 5. SEM images of (a) large-size rutile TiO₂ (starting material), (b) K₂Ti₄O₉, (c) H₂Ti₄O₉ and (d) non-doped TiO₂(B) particles.

per volume is clearly owing to their high tap densities and high electrode densities. In addition, the Nb-doped samples exhibited good cycleability, comparable with that of the conventional TiO₂(B). The discharge capacity of 197 mAh g⁻¹ (221 mAh cm⁻³) was kept even in the 50th cycle especially for Ti_{0.90}Nb_{0.10}O₂(B), which is higher than the theoretical capacity of the LTO negative electrode (175 mAh g⁻¹).

For each sample, a relatively large irreversible capacity was observed in the first cycle. This is due to the solvent decomposition in the first charging process as discussed in a previous paper [17].

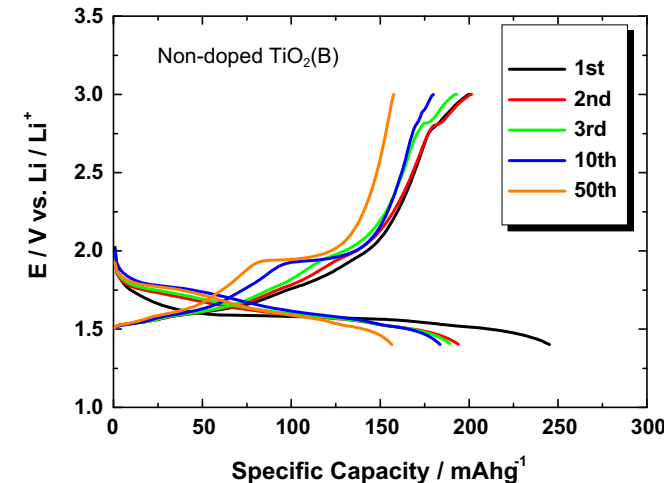


Fig. 6. Charge and discharge curves of non-doped TiO₂(B) prepared with large-size rutile TiO₂ powder as a starting material between 1.4 and 3.0 V at C/6 in 1 M LiPF₆/EC + DEC(1:1).

The Coulombic efficiency in the first cycle was hence not so high (83–88%) for each sample; however, it was not significantly affected by Nb-doping.

3.3. Effects of Nd-doping

To investigate the effects of Nb-doping in more detail, non-doped rutile TiO₂ particles were prepared by heating the anatase TiO₂ particles at 1350 °C for 10 h, and non-doped TiO₂(B) was synthesized using the non-doped rutile TiO₂ as a raw material in a

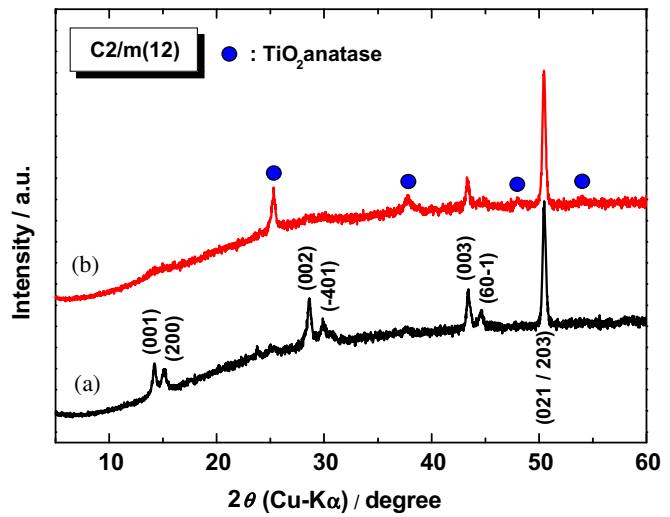


Fig. 7. XRD patterns of the composite electrode of the non-doped TiO₂(B) (a) before cycling and (b) after 50 cycles between 1.4 and 3.0 V at C/6 in 1 M LiPF₆/EC + DEC(1:1).

similar manner. Fig. 5 shows SEM images of the TiO₂ (starting material), precursor, protonated precursor and dehydrated powder. The particle size of the starting material (rutile TiO₂) was large (5–20 µm) as well as the Nb-doped one (Fig. 2(b)). The morphology of the K₂Ti₄O₉ precursor was very similar to that of the K₂Ti_{3.72}Nb_{0.28}O₉ precursor shown in Fig. 3(a). Very fine primary particles were agglomerated to form large secondary particles. Therefore the reaction mechanism for the precursor formation is the same as that for the Nb-doped one; that is, K⁺ ions penetrated into the large rutile TiO₂ particles and the fine precursor particles were formed inside. However, the agglomerated secondary particles completely decomposed after the ion-exchange process, and the resulting TiO₂(B) powder was very fine needle-like particles without agglomeration. The tap density and electrode density of the non-doped TiO₂(B) prepared by the new method are listed in Table 1. They were also higher than that of the conventional TiO₂(B) and were comparable with those of the Nb-doped samples. The formation of the large secondary particles in the final dehydrated products is one of the effects of Nb-doping as shown in Fig. 3(c); however, it is considered that the main reason for the high tap density and high electrode density originated not from the presence of the secondary particles, but from the small size of the primary particles.

Fig. 6 shows charge and discharge curves of the non-doped TiO₂(B) in 1 M LiPF₆/EC + DEC(1:1). The first discharge capacities per weight and volume were 200 mAh g⁻¹ and 202 mAh cm⁻³, respectively, which were comparable with those of the Nb-doped samples. However, upon repeated cycles, new plateaus appeared at ca. 1.75 V and 1.90 V, respectively, which are assigned to the Li insertion and extraction reactions of the anatase TiO₂ phase [20,21]. In addition, deterioration of the charge and discharge capacities upon cycling was clearly observed. Fig. 7 compares the XRD patterns of the non-doped TiO₂(B) electrode before cycling and after 50 cycles. After 50 cycles, the peaks assigned to TiO₂(B) disappeared and the peaks assigned to the anatase phase were clearly observed. This fact suggests that Nb-doping has a positive effect for stabilization of TiO₂(B) structure of the fine Nb-doped TiO₂(B) particles, though further investigation is needed to clarify the mechanism for the stabilization. As a result, Nb-doping gave good cycleability to the Nb-doped TiO₂(B) samples.

4. Conclusions

We found that the use of large-size Nb-doped rutile TiO₂ particles as a starting material greatly changes the shape and size of the resulting Nb-doped TiO₂(B) powder. The resulting Nb-doped TiO₂(B) particles were much smaller than that of the conventional TiO₂(B), and were agglomerated to form secondary particles with a diameter of 3–30 µm. The tap density successfully increased for Ti_{0.93}Nb_{0.07}O₂(B) and Ti_{0.90}Nb_{0.10}O₂(B), (0.77 and 0.66 g cm⁻³,

respectively), which were ca. 2-fold higher than that of the conventional TiO₂(B) (0.30 g cm⁻³). As a result, the discharge capacity per electrode volume was significantly improved for both Nb-doped samples without sacrificing the cycleability. Non-doped TiO₂(B) was also prepared from large-size non-doped rutile TiO₂ as a starting material, and the effect of Nb-doping was investigated. The non-doped TiO₂(B) powder was also smaller than that prepared by the conventional method using fine anatase powder as a starting material, and showed a high discharge capacity per electrode volume. However it deteriorated to form the anatase phase upon cycling. It was shown that Nb-doping not only improves the discharge capacity per electrode volume, but also effectively stabilizes the TiO₂(B) crystal structure of the small particles. The reason for the structural improvement by Nb-doping is not clear at present, and are now under investigation.

Acknowledgment

This work was supported by “The Kyoto Environmental Nanotechnology Cluster” from MEXT, Japan.

References

- [1] B. Scrosati, Nature 373 (1995) 557.
- [2] K.M. Colbow, J.R. Dahn, R.R. Haering, J. Power Sources 26 (1989) 397.
- [3] T. Ohzuku, A. Ueda, N. Yamamoto, J. Electrochem. Soc. 142 (1995) 1431.
- [4] K. Zaghib, M. Simoneau, M. Armand, M. Gauthier, J. Power Sources 81 (1999) 300.
- [5] C. Jiang, M. Wei, Z. Qi, T. Kudo, I. Honma, H. Zhou, J. Power Sources 166 (2007) 239.
- [6] J.W. Kang, D.H. Kim, V. Mathew, J.S. Lim, J.H. Gim, J. Kim, J. Electrochem. Soc. 158 (2) (2011) A59.
- [7] A.R. Armstrong, G. Armstrong, J. Canales, P.G. Bruce, Angew. Chem. Int. Ed. 43 (2004) 2286.
- [8] A.R. Armstrong, G. Armstrong, J. Canales, R. Garcia, P.G. Bruce, Adv. Mater. 17 (2005) 862.
- [9] A.R. Armstrong, G. Armstrong, J. Canales, P.G. Bruce, J. Power Sources 146 (2005) 501.
- [10] G. Armstrong, A.R. Armstrong, J. Canales, P.G. Bruce, Chem. Commun. 2454 (2005).
- [11] G. Armstrong, A.R. Armstrong, J. Canales, P.G. Bruce, Electrochem. Solid State Lett. 9 (2006) A139.
- [12] H. Zhang, G.R. Li, L.P. An, T.Y. Yan, X.P. Gao, H.Y. Zhu, J. Phys. Chem. C 111 (2007) 6143.
- [13] L.P. An, X.P. Gao, G.R. Li, T.Y. Yana, H.Y. Zhub, P.W. Shen, Electrochim. Acta 53 (2008) 4573.
- [14] C. Arrouvel, S.C. Parker, M.S. Islam, Chem. Mater. 21 (2009) 4778.
- [15] G. Armstrong, C. Arrouvel, V. Gentili, S.C. Parker, M.S. Islam, P.G. Bruce, Chem. Mater. 22 (2010) 6426.
- [16] M. Inaba, Y. Oba, F. Niina, Y. Murota, Y. Ogino, A. Tasaka, K. Hirota, J. Power Sources 189 (2009) 580.
- [17] Y. Murota, Y. Oba, M. Takagi, T. Asao, M. Saito, A. Tasaka, M. Inaba, Electrochemistry 78 (5) (2010) 431.
- [18] M. Saito, Y. Murota, M. Takagi, T. Asao, H. Inoue, A. Tasaka, M. Inaba, J. Electrochem. Soc. 159 (1) (2012) A49.
- [19] N. Kumagai, D. Yoshikawa, Y. Kadoma, K. Ui, Electrochemistry 78 (2010) 754.
- [20] M. Wagemakers, R. van de Krol, A.P.M. Kentgens, A.A. van Well, F.M. Mulder, J. Am. Chem. Soc. 123 (2001) 11454.
- [21] M. Wagemakers, A.P.M. Kentgens, F.M. Mulder, Nature 418 (2002) 397.